ACS NANO

www.acsnano.org

ARTICLE

# Insights into Self-Assembly of Nonplanar Molecules with Aggregation-Induced Emission Characteristics

Jie Li,[#] Jianyu Zhang,[#] Jianxing Wang, Dong Wang,* Yun Yan,* Jianbin Huang,* and Ben Zhong Tang*

Cite This: *ACS Nano* 2022, 16, 20559–20566

Read Online

ACCESS | Metrics & More | Article Recommendations | Supporting Information

**ABSTRACT:** **Utilizing nonplanar conjugated molecules as building blocks facilitates the development of self-assembly but is fundamentally challenging. To study the self-assembly behavior, we herein demonstrate the self-assembly process of a nonplanar conjugated molecule with aggregation-induced emission (AIE) feature from an isolated molecule to an irregular cluster to a well-defined vesicle driven by amphiphiles. The superhigh aggregation-sensitive emission affords more precise and detailed information about the self-assembly process than traditional dyes. Meanwhile, the arrangements of the AIE-active molecule change from disordered to well-organized forms by reducing the twisted configuration during the transformation process, and the strong hydrophobicity of amphiphiles is crucial for such configuration and morphology transformations. Owing to the thermophilic bacteria-mimetic membranes, the obtained vesicles exhibit a property of superhigh thermal stability. They also display promising light-harvesting applications. This work not only deciphers the self-assembly of AIE molecules but also provides a strategy for nonplanar molecules to build well-organized self-assemblies.**

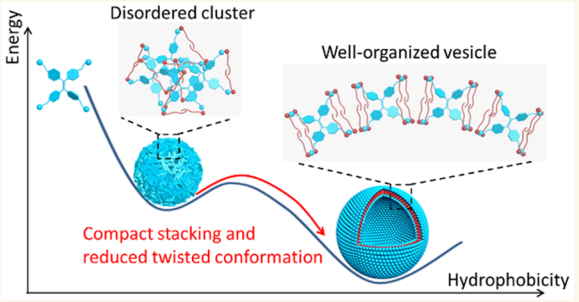


**KEYWORDS:** *aggregation-induced emission, self-assembly, nonplanar, vesicles, thermostable*

## INTRODUCTION

Nonplanar conjugated molecules present a large class of conjugated molecules with highly twisted or bent conformations.[1−6] They usually exhibit impressive performances in luminescence, electronics, and chirality that are obviously different from traditional planar conjugated molecules.[7−14] However, nonplanar conjugated molecules are rarely exploited as building blocks for self-assembly because their nonplanar configurations spatially prevent the intermolecular orientation and stacking, often resulting in disordered or amorphous architectures. In addition, although some self-assemblies have been successfully constructed by nonplanar conjugated molecules, the related self-assembly principles still remain unclear.[15−18] Therefore, to extend the building blocks of self-assembly and prompt the development of material science, investigating the self-assembly behaviors of nonplanar conjugated molecules is supremely significant.

A noteworthy feature of nonplanar conjugated molecules is the altered molecular conformations upon aggregation, which always induces prominent variation to luminescence, such as intensity and wavelength.[19−26] The special examples are aggregation-induced emission (AIE)-active molecules that have twisted configurations. They display fantastic aggregation-sensitive emission resulting from the restrained intramolecular motions.[27−31] Compared with the dispersed state, the intensity of aggregates can be enhanced hundreds of times, which is definitely opposite to the aggregation-caused quenching (ACQ) effect of traditional dyes.[32−35] Such distinct nature in fluorescence endows AIE-active molecules with great possibilities for the precise and detailed information on the self-assembly process, including molecular configurations, orientations, and intermediates.[36−38] This could be used as a quite simple and promising approach of fluorescence spectrometry for in-depth insights into the self-assembly behaviors of nonplanar conjugated molecules.

Herein, we investigated the self-assembly process of AIE-active molecules from dispersed molecules to vesicular structures based on demonstrating the coassembling behaviors of AIE-active molecule TPE-BPA and cetyltrimethylammonium bromide amphiphile (CTAB) (Figure 1A). By adopting

Received: July 21, 2022
Accepted: November 11, 2022
Published: November 16, 2022

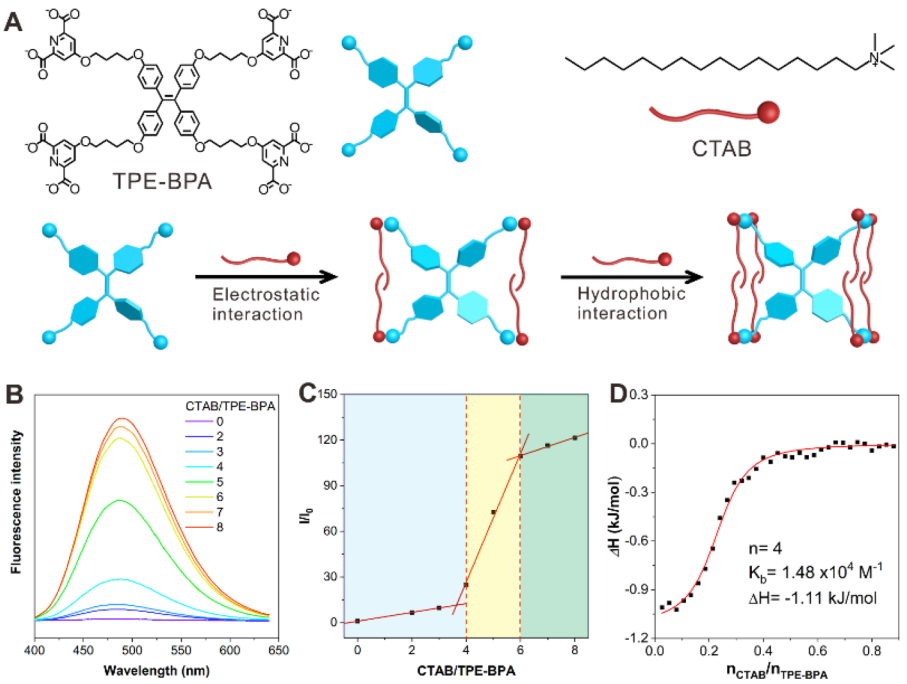


**Figure 1. (A) Chemical structures of TPE-BPA and CTAB, and their binding interactions. (B) Fluorescence spectra and (C) intensity enhancement of TPE-BPA with increasing fractions of CTAB. $I_0$ is fluorescence intensity at CTAB/TPA-BPA = 0, [TPE-BPA] = 25 $\mu$M. (D) ITC result of TPE-BPA in the presence of CTAB.**

CTAB to progressively assemble TPE-BPA, each intermediate in the self-assembly process was evaluated, and a successive morphological evolution from oligomers to irregular clusters, well-defined nanosheets, and vesicles was observed. More importantly, strong hydrophobicity mainly drove the transformation from disordered clusters to well-organized vesicles, where TPE-BPA reduced its dihedral angles for the ordered arrangement. Vesicles could be also obtained by utilizing amphiphiles with stronger hydrophobicity than CTAB, while clusters were produced with the use of amphiphiles with weaker hydrophobicity. Furthermore, the obtained vesicles were stable in heat conditions because of the thermophilic bacteria-mimetic single-layer structure of TPE-BPA in membranes. They also served as excellent candidates for light-harvesting applications because of the high quantum yield (QY) of 42%.

## RESULTS AND DISCUSSION

In the chemical structure of TPE-BPA, four hydrophilic chelidamic acid groups were attached to the AIE-active segment tetraphenylethylene[39−41] (Figure 1A). Such structure endowed TPE-BPA with 8 negative charges, which not only renders TPE-BPA with excellent solubility in water but also offers potential capacity to combine positively charged amphiphiles for assembling. Fluorescent spectra showed that TPE-BPA had negligible emission in water but emitted intensely upon addition of poor solvent (Figure S1). Dynamic light scattering (DLS) result and transmission electron microscope (TEM) image showed that TPE-BPA formed aggregates at DMF fraction of 95% (Figure S2). These solidly indicated the AIE feature of TPE-BPA. Moreover, the intensity enhancement was up to 100 times when the fraction of poor solvent was 95%. This "turn-on" emission was more obvious than that of traditional dyes, and it could offer more information about the self-assembly process of AIE molecules.

It was demonstrated that TPE-BPA bound 8 CTAB to self-assemble into a well-defined vesicular structure.[36−38] Therefore, we studied the self-assembly process by stepwise addition of CTAB into TPE-BPA aqueous solution in terms of the hydrophobicity of CTAB. The fluorescence intensities gradually increased when the molar ratios of CTAB/TPE-BPA increased, indicating the aggregating process of TPE-BPA (Figure 1B). The fluorescence intensity at the molar ratio of 8 was enhanced to 120 times by comparison with free TPE-BPA. Compared with traditional planar dyes that have emission intensity variations with several times, such superhigh aggregation-sensitive emission could be used to validate the self-assembly process of vesicles. As illustrated in Figure 1C, the emission intensity underwent a slight enhancement at the molar ratios ranging from 0 to 4, and it drastically boosted when the molar ratios altered from 5 to 6. Then the intensity increased mildly again from molar ratio of 7 to 8. This change was consistent with variations of QY (Figure S3), suggesting that there were three stages in the self-assembly process of vesicles. The variation of scattering light intensities indicated that there were possibly four morphologies of aggregates in the self-assembly process (Figure S4). Moreover, the isothermal titration calorimetry (ITC) result in Figure 1D displayed that the best binding ratio of CTAB/TPA-BPA was 4, in which the corresponding binding constant and enthalpy were $1.48 \times 10^4$ $M^{-1}$ and −1.11 kJ/mol, respectively. This revealed that TPA-BPA combined with 4 CTAB through electrostatic interaction to form a thermodynamically stable intermediate, which consequently bound more CTAB than that mainly driven by a hydrophobic interaction (Figure 1A). Meanwhile, the binding interaction of the intermediate was tested by mixing different charged amphiphiles with TPA-BPA (Figure S5). The treatment of positively charged amphiphiles induced bright fluorescence while faint emissions were detected upon mixing


https://doi.org/10.1021/acsnano.2c07263
ACS Nano 2022, 16, 20559−20566

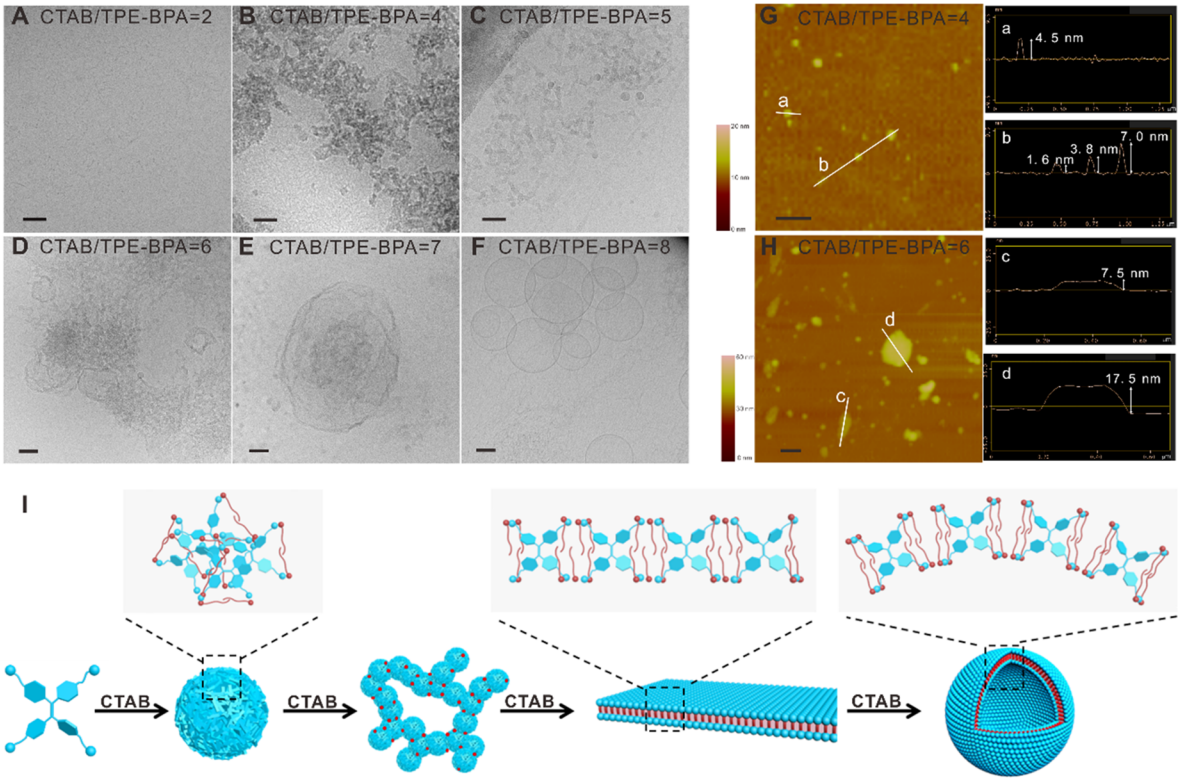


**Figure 2.** (A–F) TEM images of aggregates at various CTAB/TPE-BPA ratios. Scale bars are 50 nm. (G,H) AFM imaging and height analysis of aggregates at CTAB/TPE-BPA ratios of 4 and 6. Scale bars are 200 nm. (I) Schematic illustration of self-assembly process of TPE-BPA with CTAB. [TPE-BPA] = 25 $\mu$M.

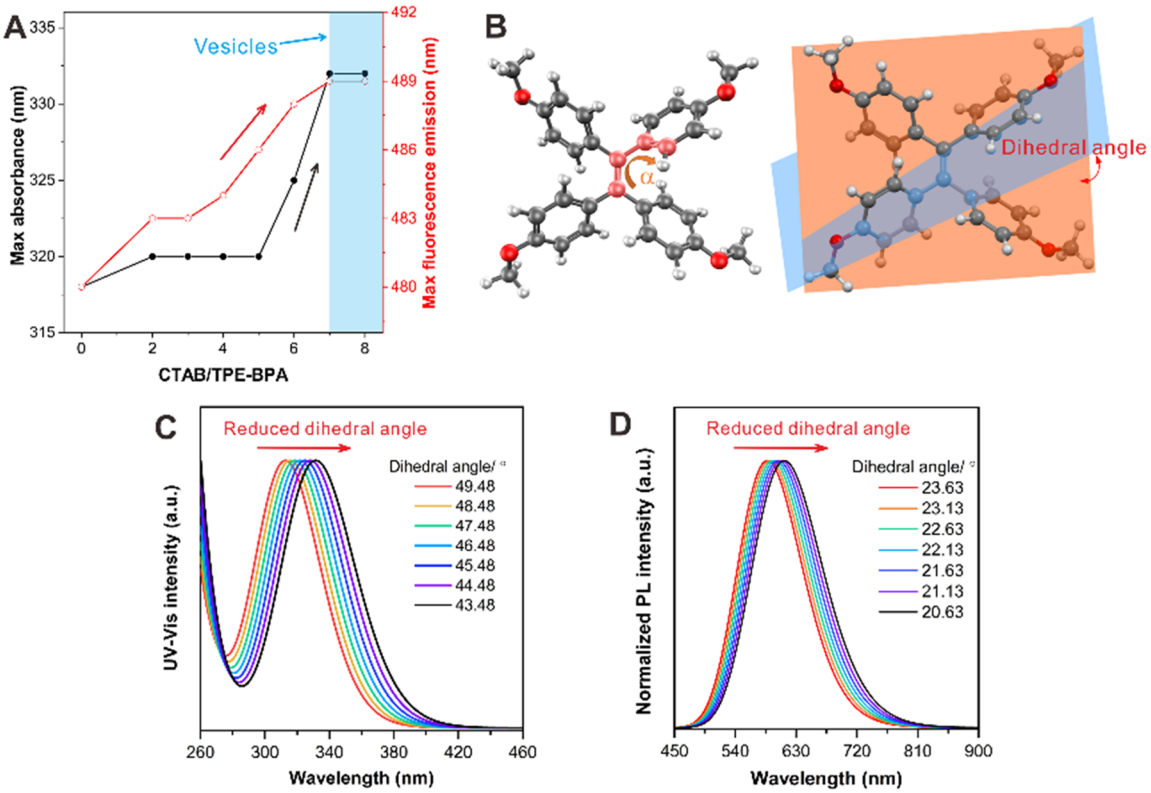


**Figure 3.** (A) Variation of absorbance and emission wavelengths of TPE-BPA with different ratios of CTAB. [TPE-BPA] = 25 $\mu$M. (B) Molecular configuration of TMPE and the dihedral angle. Calculated absorbance (C) and emission (D) of TMPE with altered dihedral angles.



https://doi.org/10.1021/acsnano.2c07263
ACS Nano 2022, 16, 20559–20566

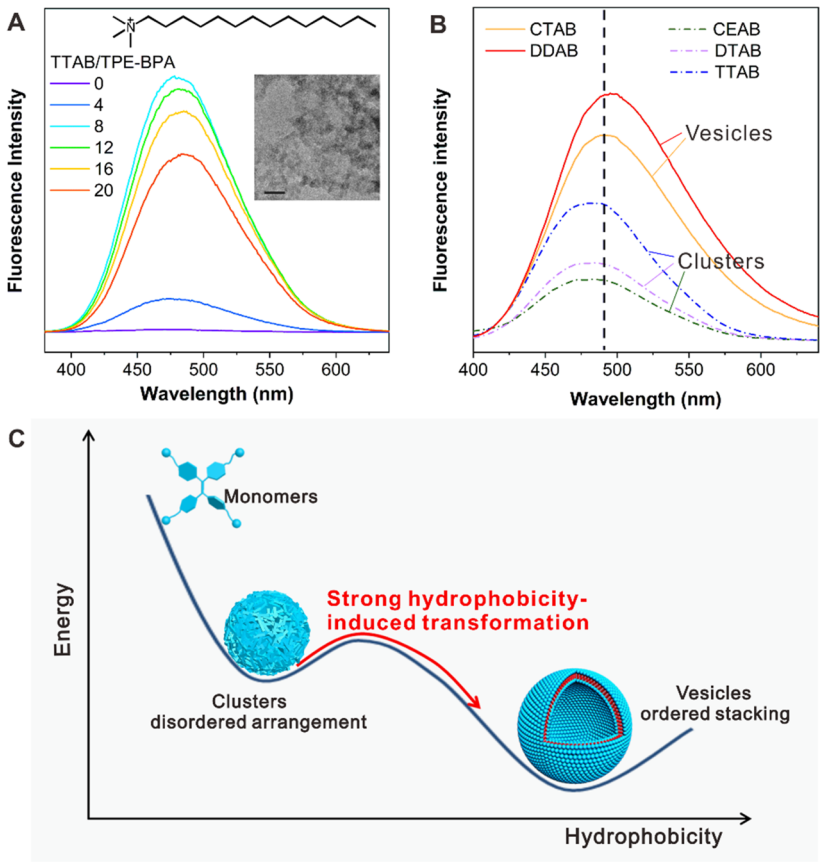


**Figure 4. (A) Fluorescence emission of TPE-BPA with different ratios of TTAB. Insets are the chemical structure of TTAB and the TEM image of 8TTAB@TPE-BPA. Scale bar is 100 nm. (B) Fluorescence emission of TPE-BPA with different amphiphiles. [TPE-BPA] = 25 $\mu$M. (C) Schematic illustration of transformation from monomers to clusters to vesicles with amphiphiles.**

with negatively charged or uncharged ones, verifying the electrostatic interaction for the intermediates.

To further monitor the self-assembly process, the aggregates in three stages were investigated by TEM, DLS, atomic force microscope (AFM), and fluorescent lifetime. Although no signal was detected in DLS results in the first stage in which the molar ratios of CTAB/TPE-BPA were less than 3, the clearly increased lifetimes of TPE-BPA upon combining with CTAB (Figure S6A) and aggregates with ambiguous contrast in TEM image (Figure 2A) demonstrated the formation of incompact oligomers.[42] When the molar ratio reached 4, obvious aggregates with a diameter of 40 nm were observed (Figure S7). These aggregates not only had irregular shapes (Figure 2B), but also demonstrated various thicknesses of 1.6, 3.8, 4.5, and 7.0 nm (Figure 2G) that did not match the lengths of both molecules (the lengths of TPE-BPA and CTAB were respectively 2.5 and 2.0 nm as shown in Figure S8). These outcomes indicated the morphology of irregular clusters with disordered intermolecular packing. Moreover, in the second stage, both TEM images (Figure 2C) and AFM results (Figure S9) demonstrated the formation of jointed aggregates at the molar ratio of 5, and the thicknesses of those aggregates were irregular as well, suggesting their cross-linked clusters features. Most interestingly, nanosheet structure was detected after increasing the molar ratios to 6 (Figure 2D and S10), and the nanosheets showed well-organized thicknesses that were multiple times the length of TPE-BPA (Figure 2H). Thus, according to the molecular lengths, it seemed reasonable to infer that TPE-BPA stacked regularly in the nanosheets and served as skeleton with single-layered structure, while CTAB crossed with each other with bilayer configuration (Figure 2I). With further addition of CTAB in the third stage of self-assembly, irregular vesicles with a diameter of 100 nm at a molar ratio of 7 and well-defined vesicular structure at molar ratio of 8 were found (Figure 2E,F). The thicknesses of these vesicles were even times the length of TPE-BPA (Figures S11 and S12), illustrating the hollow architectures and the same ordered molecular packing in membrane as the nanosheets. This demonstrated that irregular and well-defined vesicles were converted by nanosheets. Additionally, lifetimes continuously increased during the whole processes (Figure S6), showing that TPE-BPA packed more and more tensely, and this might be ascribed to the hydrophobicity of CTAB.

Considering the above results, the self-assembly process of vesicles can be illustrated as Figure 2I: electrostatic interaction dominated the integration of TPE-BPA with 4 CTAB to form clusters with disordered arrangement, then the clusters cross-linked together to build nanosheets and further transferred into vesicles by combining more CTAB, where TPE-BPA and CTAB organized regularly.

As most aggregates fabricated by AIE-active molecules held disordered stacking and undefined morphologies resulted from the twisted conformation,[43,44] it was quite exciting that irregular clusters transferred into well-defined vesicular structure in this contribution. In this regard, studying this transferring process could afford deep insights into the self-assembly behaviors of AIE-active molecules. As shown in Figures 3A and S13, redshifts of both UV absorbance and


https://doi.org/10.1021/acsnano.2c07263
ACS Nano 2022, 16, 20559−20566

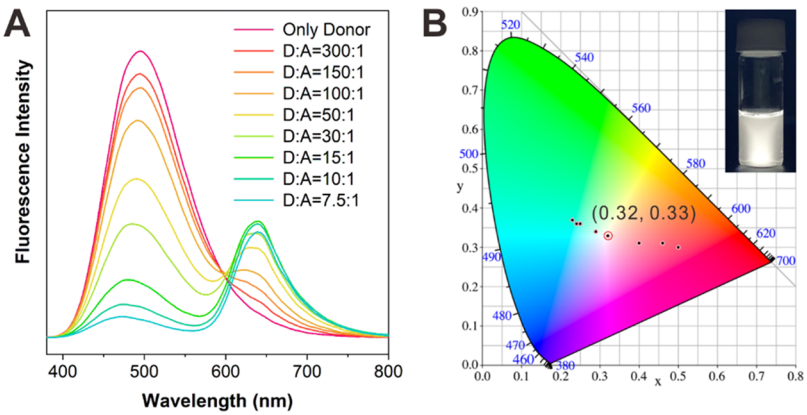


**Figure 5. (A) Fluorescence emission of vesicles with addition of acceptors NiR. D: A presents the molar ratios of TPE-BPA (donor) and NiR (acceptor). (B) CIE chromaticity diagram of vesicles with different proportions of NiR. Insert is the photo of white-emissive vesicle solution under 365 nm lamp. [TPE-BPA] = 25 $\mu$M, [CTAB] = 200 $\mu$M.**

fluorescence emission occurred in the transformation process from clusters to vesicles, accompanied by enhanced QY and prolonged lifetime of TPE-BPA. This suggested the change of molecular configuration and restriction of the molecular motions. To evaluate whether restrained molecular motions contributed the redshifts, the fluorescence emissions of bare TPE-BPA in aqueous solution at different temperature were detected (Figure S14). TPE-BPA could rotate freely and exhibited negligible emission located at 478 nm at room temperature. Upon exposure to a frozen water condition (77K) to prohibit the molecular motions, TPE-BPA emitted brightly with the maximum emission of 467 nm. Such blueshift indicated that the redshifts observed in the self-assembly process were mainly ascribed to the altered molecular configurations. To validate the relationship between molecular configuration and wavelength shifts of absorbance and emission, theoretical calculation was conducted by adopting tetrakis(4-methoxyphenyl)ethylene (TMPE) as a simplified model for TPE-BPA, since TMPE was the AIE-active segment of TPE-BPA and they had almost the same twisted confirmation and energy gaps (Figure S15 and Table S1). The dihedral angles caused by torsion between double bond and phenyl groups significantly contributed the nonplanar configuration of TMPE and TPE-BPA, which hampered the ordered arrangement and self-assembly (Figure 3B). Calculated results in Figure 3C,D revealed that gradual redshifts of both absorbance and emission wavelengths generally resulted in diminishing dihedral angles, demonstrating that TPA-BPA decreased the dihedral angles in transformation process from clusters to vesicle. This was because decreased dihedral angles could efficiently weaken the steric hindrance and prompt the ordered staking of TPE-BPA, consequently rendering the formation of well-defined structures.

The addition of CTAB drove the transformation from clusters to vesicles; thereby, the role of positive amphiphiles was explored. Tetradecyltrimethylammonium bromide (TTAB) was a positive amphiphile that had weaker hydrophobicity than CTAB because its shorter alkyl chain. With stepwise introduction of TTAB into a TPA-BPA solution, the fluorescence intensity progressively increased and reached the maximum at the molar ratio of 8, but reduced with further addition of TTAB (Figure 4A). This suggested that the optimal molar ratio of TTAB/TPE-BPA was 8 where the TPE-BPA packed the most tensely and held the largest possibility for ordered arrangement. However, TEM image clearly presented the irregular clusters at the optimal molar ratio (8TTAB@TPE-BPA), indicating that TTAB@TPE-BPA system could not form vesicles. Moreover, the same results were found after integrating other positive amphiphiles dodecyltrimethylaminium bromide (DTAB) and cetyltriethylammonium bromide (CEAB) with weaker hydrophobicity than CTAB (Figure S16 and S17). Fortunately, vesicles were produced at the optimal molar ratio by exploiting positive amphiphile didodecyldimethylammonium bromide (DDAB) with stronger hydrophobicity than CTAB (Figure S18).[45] Meanwhile, at the optimal molar ratios, the TPE-BPA solution with treatment of DDAB and CTAB showed higher fluorescence intensity and larger redshifts of emission than that of DTAB, CEAB, and TTAB, revealing more tense stacking and smaller dihedral angles of TPE-BPA in vesicular structure than that in clusters (Figure 4B). These results indicated that only strong enough hydrophobicity could endow TPE-BPA with compact packing to reduce the dihedral angles accompanying with diminished steric hindrance, and the clusters could convert into vesicles (Figure 4C), which manifested the crucial role of hydrophobicity for transferring clusters into vesicles.

The membrane of thermophilic bacteria mainly comprises a specific phospholipid with two hydrophilic groups at the ends that self-assembles with transmembrane and single-layer manners. This architecture keeps bacterial membranes stable in heat conditions and contributes the heat resistance.[46,47] With regards to the single-layer structure of TPE-BPA in the membrane of 8CTAB@TPE-BPA vesicles, the vesicles would possess great possibilities of thermal stability as thermophilic bacteria. Differential scanning calorimeter (DSC) test demonstrated no changes when the temperature varied from 20 to 80 °C, indicating that no phase transition occurred (Figure S19A). Moreover, the size of vesicles did not alter in heat environments (Figure S19B). Nuclear magnetic resonance (NMR) results further displayed the linear shifts of proton in TPE-BPA upon gradually increasing temperatures, revealing that no variation occurred in microenvironments (Figure S20). Furthermore, the vesicles also exhibited strong emission at high-temperature conditions (Figure S21). These solidly suggested that 8CTAB@TPE-BPA vesicles were thermally stable and could also conversely confirmed the single-layer structure in membrane.


https://doi.org/10.1021/acsnano.2c07263
ACS Nano 2022, 16, 20559−20566

Different from the traditional planar conjugated molecules that suffered aggregation-caused quenching, AIE molecules usually possessed impressively enhanced fluorescence in assemblies.[27−31] Such merit rendered 8CTAB@TPE-BPA vesicles with a superhigh QY of 42% and could serve as excellent donors for light harvesting materials. Hydrophobic Nile red (NiR) dye was chosen as the acceptor on account that it could adhere to the hydrophobic area of vesicle membranes, and its absorbance was largely overlaid with the emission of the vesicle (Figure S22A). As illustrated in Figure 5A, the vesicles displayed intensive emission at 490 nm, and the intensity progressively diminished upon stepwise addition of NiR, while the emission of NiR at 630 nm simultaneously increased. This indicated the energy conversion from donors (vesicles) to acceptors (NiR). Meanwhile, the average lifetime of TPE-BPA in vesicles was 1.966 ns, and it became 0.327 ns when the molar ratio of donor/acceptor was 7.5:1, which confirmed the energy conversion through the Förster resonance energy transfer (FRET) process.[48−50] The corresponding energy transfer efficiency was calculated to be 83% according to the fluorescence lifetimes (Figure S22B), where the antenna effect value was calculated to be 0.95 in water (Figure S23). Additionally, the fluorescence emission of vesicles can be easily tuned from green to red through FRET process, and white light-emissive vesicles with Commission Internationale de l'Éclairage (CIE) 1931 coordinate of (0.32, 0.33) was also successfully obtained at the D/A ratio of 30:1 (Figure 5B). Furthermore, adding NiR did not change the size and morphologies of vesicles (Figure S24). These revealed that the vesicle@NiR was a promising light-harvesting system.

## CONCLUSION

In conclusion, we have successfully presented the self-assembly process of vesicles fabricated by an AIE-active molecule TPE-BPA with twisted configuration and amphiphile CTAB. It was clearly observed that TPE-BPA bound with CTAB to form the stable intermediates with disordered arrangement, and the disordered aggregates consequently cross-linked and transferred to vesicles with ordered stacking. In the morphological transition, hydrophobic effect must be strong enough to render TPE-BPA pack tensely and consequently reduce the dihedral angles to weaken the steric hindrance, which could result in the ordered stacking for self-assembly. The obtained vesicle showed thermal stability in aqueous solution, mainly benefiting from the thermophilic bacteria-mimetic single-layer structure in membrane. In addition, the vesicles were excellent candidates for light-harvesting and white-emissive systems due to impressively high emission intensity. We hope that this study could facilitate an understanding of the self-assembly principles of AIE molecules and afford strategies for constructing self-assemblies by nonplanar molecules at will.

## EXPERIMENTAL SECTION

**Method.** The TPE-BPA contained self-assemblies were prepared as follow: 15 μL of a TPE-BPA aqueous solution (5 mM) and desired amounts of amphiphiles (10 mM) were directly mixed, then water was added to reach a total volume of 3 mL. The obtained solutions were stirred for 1 min and kept at room temperature for 24 h before use.

**Isothermal Titration Calorimetry (ITC).** The calorimetric measurements were conducted on a TAM 2277−201 microcalorimetric system (Thermometric AB, Järfälla, Sweden) with a stainless-steel sample cell of 1 mL at 25.00 ± 0.01 °C. The sample cells were initially loaded with 600 μL of water or 0.05 mM TPE-BPA solution, and then CTAB solution (8 mM) was injected consecutively into the stirred sample cell in portions of 10 μL via a 500 μL Hamilton syringe controlled by a 612 Thermometric Lund pump until the end of the interaction. The system was stirred at 60 rpm with a gold propeller.

**Transmission Electron Microscope (TEM).** A drop of sample solution (~4 μL) was dropped on a grid in a high humidity environment (>90%). The excess sample was blotted up by two pieces of blotting paper, leaving a thin film sprawling on the grid. Then the grid was plunged into liquid ethane, which was frozen by liquid nitrogen. The vitrified sample was transferred into a sample holder (Gatan 626) and observed on a JEOL JEM-1400 TEM (120 kV) at about −174 °C. The images were recorded on a Gatan multiscan CCD.

## ASSOCIATED CONTENT

### Supporting Information

The Supporting Information is available free of charge at https://pubs.acs.org/doi/10.1021/acsnano.2c07263.

Measurements and additional data, TEM and AFM images, NMR, DSC and calculated results (PDF)

## AUTHOR INFORMATION


### Corresponding Authors

**Dong Wang** − *Center for AIE Research, Shenzhen Key Laboratory of Polymer Science and Technology, College of Materials Science and Engineering, Shenzhen University, Shenzhen, Guangdong 518060, China;* orcid.org/0000-0001-5137-0771; Email: wangd@szu.edu.cn

**Yun Yan** − *Beijing National Laboratory for Molecular Sciences (BNLMS), College of Chemistry and Molecular Engineering, Peking University, Beijing 100871, China;* orcid.org/0000-0001-8759-3918; Email: yunyan@pku.edu.cn

**Jianbin Huang** − *Beijing National Laboratory for Molecular Sciences (BNLMS), College of Chemistry and Molecular Engineering, Peking University, Beijing 100871, China;* Email: jbhuang@pku.edu.cn

**Ben Zhong Tang** − *School of Science and Engineering, Shenzhen Institute of Aggregate Science and Technology, The Chinese University of Hong Kong, Shenzhen, Guangdong 518172, China;* orcid.org/0000-0002-0293-964X; Email: tangbenz@cuhk.edu.cn

### Authors

**Jie Li** − *Beijing National Laboratory for Molecular Sciences (BNLMS), College of Chemistry and Molecular Engineering, Peking University, Beijing 100871, China; Center for AIE Research, Shenzhen Key Laboratory of Polymer Science and Technology, College of Materials Science and Engineering, Shenzhen University, Shenzhen, Guangdong 518060, China*

**Jianyu Zhang** − *Hong Kong Branch of Chinese National Engineering Research Center for Tissue Restoration and Reconstruction, Department of Chemistry, The Hong Kong University of Science and Technology, Hong Kong 999077, China;* orcid.org/0000-0002-5213-7063

**Jianxing Wang** − *Center for AIE Research, Shenzhen Key Laboratory of Polymer Science and Technology, College of Materials Science and Engineering, Shenzhen University, Shenzhen, Guangdong 518060, China*

Complete contact information is available at: https://pubs.acs.org/10.1021/acsnano.2c07263

### Author Contributions

#J.L. and J.Z. contributed equally.




https://doi.org/10.1021/acsnano.2c07263
ACS Nano 2022, 16, 20559−20566

## Notes

The authors declare no competing financial interest.

## ACKNOWLEDGMENTS

This work was financially supported by the National Natural Science Foundation of China (52122317, 22175120, 21902106, 22172004, 21972003), and the Developmental Fund for Science and Technology of Shenzhen Government (JCYJ20190808153415062, RCYX20200714114525101), the Natural Science Foundation for Distinguished Young Scholars of Guangdong Province (2020B1515020011).

## REFERENCES

(1) Ueda, M.; Jorner, K.; Sung, Y. M.; Mori, T.; Xiao, Q.; Kim, D.; Ottosson, H.; Aida, T.; Itoh, Y. Energetics of Baird Aromaticity Supported by Inversion of Photoexcited Chiral [4n]annulene Derivatives. *Nat. Commun.* **2017**, *8*, 346.

(2) Sun, G.; Wei, Y.-C.; Zhang, Z.; Lin, J.-A.; Liu, Z.-Y.; Chen, W.; Su, J.; Chou, P.-T.; Tian, H. Diversified Excited-State Relaxation Pathways of Donor-Linker-Acceptor Dyads Controlled by a Bent-to-Planar Motion of the Donor. *Angew. Chem., Int. Ed.* **2020**, *59*, 18611−18618.

(3) Soya, T.; Mori, H.; Osuka, A. Quadruply Twisted Hgckel-Aromatic Dodecaphyrin. *Angew. Chem., Int. Ed.* **2018**, *57*, 15882−15886.

(4) Liu, Z.; Wang, X.; Chen, Q.; Ma, F.; Huang, Y.; Gao, Y.; Deng, Q.; Qiao, Z.-Y.; Xing, X.; Zhu, J.; Lu, F.; Wang, H. Regulating Twisted Skeleton to Construct Organ-Specific Perylene for Intensive Cancer Chemotherapy. *Angew. Chem., Int. Ed.* **2021**, *60*, 16215−16223.

(5) Nakakuki, Y.; Hirose, T.; Sotome, H.; Miyasaka, H.; Matsuda, K. Hexa-peri-hexabenzo[7]helicene: Homogeneously π-Extended Helicene as a Primary Substructure of Helically Twisted Chiral Graphenes. *J. Am. Chem. Soc.* **2018**, *140*, 4317−4326.

(6) Kotani, R.; Liu, L.; Kumar, P.; Kuramochi, H.; Tahara, T.; Liu, P.; Osuka, A.; Karadakov, P. B.; Saito, S. Controlling the $S_1$ Energy Profile by Tuning Excited-State Aromaticity. *J. Am. Chem. Soc.* **2020**, *142*, 14985−14992.

(7) Li, Q.; Li, C.; Baryshnikov, G.; Ding, Y.; Zhao, C.; Gu, T.; Sha, F.; Liang, X.; Zhu, W.; Wu, X.; Ågren, H.; Sessler, J. L.; Xie, Y. Twisted-Planar-Twisted Expanded Porphyrinoid Dimer as a Rudimentary Reaction-based Methanol Indicator. *Nat. Commun.* **2020**, *11*, 5289.

(8) Liu, G.; Xiao, C.; Negri, F.; Li, Y.; Wang, Z. Dodecatwistarene Imides with Zigzag-Twisted Conformation for Organic Electronics. *Angew. Chem., Int. Ed.* **2020**, *59*, 2008−2012.

(9) Chen, G.; Li, W.; Zhou, T.; Peng, Q.; Zhai, D.; Li, H.; Yuan, W. Z.; Zhang, Y.; Tang, B. Z. Conjugation-Induced Rigidity in Twisting Molecules: Filling the Gap Between Aggregation-Caused Quenching and Aggregation-Induced Emission. *Adv. Mater.* **2015**, *27*, 4496−4501.

(10) Zhou, C.; Ren, Y.; Han, J.; Gong, X.; Wei, Z.; Xie, J.; Guo, R. Controllable Supramolecular Chiral Twisted Nanoribbons from Achiral Conjugated Oligoaniline Derivatives. *J. Am. Chem. Soc.* **2018**, *140*, 9417−9425.

(11) Liu, S.; Ou, H.; Li, Y.; Zhang, H.; Liu, J.; Lu, X.; Kwok, R. T. K.; Lam, J. W. Y.; Ding, D.; Tang, B. Z. Planar and Twisted Molecular Structure Leads to the High Brightness of Semiconducting Polymer Nanoparticles for NIR-IIa Fluorescence Imaging. *J. Am. Chem. Soc.* **2020**, *142*, 15146−15156.

(12) Fan, W.; Matsuno, T.; Han, Y.; Wang, X.; Zhou, Q.; Isobe, H.; Wu, J. Synthesis and Chiral Resolution of Twisted Carbon Nanobelts. *J. Am. Chem. Soc.* **2021**, *143*, 15924−15929.

(13) Zhang, L.; Wang, H.-X.; Li, S.; Liu, M. Supramolecular Chiroptical Switches. *Chem. Soc. Rev.* **2020**, *49*, 9095−9120.

(14) Wang, C.; Chi, W.; Qiao, Q.; Tan, D.; Xu, Z.; Liu, X. Twisted Intramolecular Charge Transfer (TICT) and Twists beyond TICT: from Mechanisms to Rational Designs of Bright and Sensitive Fluorophores. *Chem. Soc. Rev.* **2021**, *50*, 12656−12678.

(15) Li, J.; Wang, J.; Li, H.; Song, N.; Wang, D.; Tang, B. Z. Supramolecular Materials based on AIE Luminogens (AIEgens): Construction and Applications. *Chem. Soc. Rev.* **2020**, *49*, 1144−1172.

(16) Lou, X.-Y.; Yang, Y.-W. Pyridine-Conjugated Pillar[5]arene: From Molecular Crystals of Blue Luminescence to Red-Emissive Coordination Nanocrystals. *J. Am. Chem. Soc.* **2021**, *143*, 11976−11981.

(17) Görl, D.; Zhang, X.; Stepanenko, V.; Würthner, F. Supramolecular Block Copolymers by Kinetically Controlled Co-self-assembly of Planar and Core-twisted Perylene Bisimides. *Nat. Commun.* **2015**, *6*, 7009.

(18) Wang, F.; Gan, F.; Shen, C.; Qiu, H. Amplifiable Symmetry Breaking in Aggregates of Vibrating Helical Molecules. *J. Am. Chem. Soc.* **2020**, *142*, 16167−16172.

(19) Huang, Z.; Jiang, T.; Wang, J.; Ma, X.; Tian, H. Real-Time Visual Monitoring of Kinetically Controlled Self-Assembly. *Angew. Chem., Int. Ed.* **2021**, *60*, 2855−2860.

(20) Li, J.; Wang, J.; Zhang, J.; Han, T.; Hu, X.; Lee, M. M. S.; Wang, D.; Tang, B. Z. A Facile Strategy of Boosting Photothermal Conversion Efficiency through State Transformation for Cancer Therapy. *Adv. Mater.* **2021**, *33*, 2105999.

(21) An, B.-K.; Kwon, S.-K.; Jung, S.-D.; Park, S. Y. Enhanced Emission and Its Switching in Fluorescent Organic Nanoparticles. *J. Am. Chem. Soc.* **2002**, *124*, 14410−14415.

(22) Zhang, H.; Zheng, X.; Kwok, R. T. K.; Wang, J.; Leung, N. L. C.; Shi, L.; Sun, J. Z.; Tang, Z.; Lam, J. W. Y.; Qin, A.; Tang, B. Z. In situ Monitoring of Molecular Aggregation Using Circular Dichroism. *Nat. Commun.* **2018**, *9*, 4961.

(23) Cai, S.; Chen, J.; Wang, S.; Zhang, J.; Wan, X. Allostery-Mimicking Self-assembly of Helical Poly(phenylacetylene) Block Copolymers and the Chirality Transfer. *Angew. Chem., Int. Ed.* **2021**, *60*, 9686−9692.

(24) Tu, D.; Zhang, J.; Zhang, Y.; Sung, H. H. Y.; Liu, L.; Kwok, R. T. K.; Lam, J. W. Y.; Williams, I. D.; Yan, H.; Tang, B. Z. How Do Molecular Motions Affect Structures and Properties at Molecule and Aggregate Levels? *J. Am. Chem. Soc.* **2021**, *143*, 11820−11827.

(25) Chen, W.; Guo, C.; He, Q.; Chi, X.; Lynch, V. M.; Zhang, Z.; Su, J.; Tian, H.; Sessler, J. L. Molecular Cursor Caliper: A Fluorescent Sensor for Dicarboxylate Dianions. *J. Am. Chem. Soc.* **2019**, *141*, 14798−14806.

(26) Liu, S.; Cheng, Y.; Zhang, H.; Qiu, Z.; Kwok, R. T. K.; Lam, J. W. Y.; Tang, B. Z. In Situ Monitoring of RAFT Polymerization by Tetraphenylethylene-Containing Agents with Aggregation-Induced Emission Characteristics. *Angew. Chem., Int. Ed.* **2018**, *57*, 6274−6278.

(27) Ji, X.; Li, Z.; Liu, X.; Peng, H.-Q.; Song, F.; Qi, J.; Lam, J. W. Y.; Long, L.; Sessler, J. L.; Tang, B. Z. A Functioning Macroscopic "Rubik's Cube" Assembled via Controllable Dynamic Covalent Interactions. *Adv. Mater.* **2019**, *31*, 1902365.

(28) Song, N.; Zhang, Z.; Liu, P.; Yang, Y.-W.; Wang, L.; Wang, D.; Tang, B. Z. Nanomaterials with Supramolecular Assembly Based on AIE Luminogens for Theranostic Applications. *Adv. Mater.* **2020**, *32*, 2004208.

(29) Wang, J.; Li, J.; Li, Y.; Zhang, Z.; Wang, L.; Wang, D.; Su, L.; Zhang, X.; Tang, B. Z. pH-Responsive Au(I)-disulfide Nanoparticles with Tunable Aggregation-Induced Emission for Monitoring Intragastric Acidity. *Chem. Sci.* **2020**, *11*, 6472−6478.

(30) Yan, D.; Xie, W.; Zhang, J.; Wang, L.; Wang, D.; Tang, B. Z. Donor/π-Bridge Manipulation for Constructing a Stable NIR-II Aggregation-Induced Emission Luminogen with Balanced Phototheranostic Performance. *Angew. Chem., Int. Ed.* **2021**, *60*, 26769−26980.

(31) Yan, D.; Wang, M.; Wu, Q.; Niu, N.; Li, M.; Song, R.; Rao, J.; Kang, M.; Zhang, Z.; Zhou, F.; Wang, D.; Tang, B. Z. Multimodal Imaging-Guided Photothermal Immunotherapy Based on a Versatile NIR-II Aggregation-Induced Emission Luminogen. *Angew. Chem., Int. Ed.* **2022**, DOI: 10.1002/anie.202202614.

(32) Luo, J.; Xie, Z.; Lam, J. W. Y.; Cheng, L.; Chen, H.; Qiu, C.; Kwok, H. S.; Zhan, X.; Liu, Y.; Zhu, D.; Tang, B. Z. Aggregation-

Induced Emission of 1-Methyl-1,2,3,4,5-pentaphenylsilole. *Chem. Commun.* **2001**, 1740−1741.
(33) Mei, J.; Leung, N. L. C.; Kwok, R. T. K.; Lam, J. W. Y.; Tang, B. Z. Aggregation-Induced Emission: Together We Shine, United We Soar. *Chem. Rev.* **2015**, *115*, 11718−11940.
(34) Kang, M.; Zhang, Z.; Song, N.; Li, M.; Sun, P.; Chen, X.; Wang, D.; Tang, B. Z. Aggregation-Enhanced Theranostics: AIE Sparkles in Biomedical Field. *Aggregate* **2020**, *1*, 80−106.
(35) Peng, Q.; Shuai, Z. Molecular Mechanism of Aggregation-Induced Emission. *Aggregate* **2021**, *2*, No. e91.
(36) Li, J.; Peng, K.; Li, Y.; Wang, J.; Huang, J.; Yan, Y.; Wang, D.; Tang, B. Z. Exosome-Mimetic Supramolecular Vesicles with Reversible and Controllable Fusion and Fission. *Angew. Chem., Int. Ed.* **2020**, *59*, 21510−21514.
(37) Li, J.; Shi, K.; Drechsler, M.; Tang, B. Z.; Huang, J.; Yan, Y. A Supramolecular Fluorescent Vesicle Based on a Coordinating Aggregation Induced Emission Amphiphile: Insight into the Role of Electrical Charge in Cancer Cell Division. *Chem. Commun.* **2016**, *52*, 12466.
(38) Li, J.; Liu, K.; Chen, H.; Li, R.; Drechsler, M.; Bai, F.; Huang, J.; Tang, B. Z.; Yan, Y. Functional Built-In Template Directed Siliceous Fluorescent Supramolecular Vesicles as Diagnostics. *ACS Appl. Mater. Interfaces* **2017**, *9*, 21706−21714.
(39) Zhang, N.; Chen, H.; Fan, Y.; Zhou, L.; Trépout, S.; Guo, J.; Li, M.-H. Fluorescent Polymersomes with Aggregation-Induced Emission. *ACS Nano* **2018**, *12*, 4025−4035.
(40) Peng, H.-Q.; Zheng, X.; Han, T.; Kwok, R. T. K.; Lam, J. W. Y.; Huang, X.; Tang, B. Z. Dramatic Differences in Aggregation-Induced Emission and Supramolecular Polymerizability of Tetraphenylethene-Based Stereoisomers. *J. Am. Chem. Soc.* **2017**, *139*, 10150−10156.
(41) Guan, W.; Yang, T.; Lu, C. Measurement of Solubilization Location in Micelles Using Anchored Aggregation-Induced Emission Donors. *Angew. Chem., Int. Ed.* **2020**, *59*, 12800−12805.
(42) Peng, H.-Q.; Liu, B.; Wei, P.; Zhang, P.; Zhang, H.; Zhang, J.; Li, K.; Li, Y.; Cheng, Y.; Lam, J. W. Y.; Zhang, W.; Lee, C.-S.; Tang, B. Z. Visualizing the Initial Step of Self-Assembly and the Phase Transition by Stereogenic Amphiphiles with Aggregation-Induced Emission. *ACS Nano* **2019**, *13*, 839−846.
(43) Bai, W.; Wang, Z.; Tong, J.; Mei, J.; Qin, A.; Sun, J. Z.; Tang, B. Z. A Self-assembly Induced Emission System Constructed by the Host-Guest Interaction of AIE-active Building Blocks. *Chem. Commun.* **2015**, *51*, 1089−1091.
(44) Wang, D.; Lee, M. M. S.; Xu, W.; Shan, G.; Zheng, X.; Kwok, R. T. K.; Lam, J. W. Y.; Hu, X.; Tang, B. Z. Boosting Non-Radiative Decay to Do Useful Work: Development of a Multi-Modality Theranostic System from an AIEgen. *Angew. Chem., Int. Ed.* **2019**, *58*, 5628−5632.
(45) Li, J.; Lee, M. M. S.; Li, H.; Tong, C.; Huang, J.; Yan, Y.; Wang, D.; Tang, B. Z. Programmed Self-Assembly of Protein-Coated AIE-Featured Nanoparticles with Dual Imaging and Targeted Therapy to Cancer Cells. *ACS Appl. Mater. Interfaces* **2020**, *12*, 29641−29649.
(46) Li, S.; Zheng, F.; Zhang, X.; Wang, W. Stability and Rupture of Archaebacterial Cell Membrane: A Model Study. *J. Phys. Chem. B* **2009**, *113*, 1143−1152.
(47) Yan, Y.; Huang, J.; Li, Z.; Ma, J.; Fu, H.; Ye, J. Vesicles with Superior Stability at High Temperature. *J. Phys. Chem. B* **2003**, *107*, 1479−1482.
(48) Huo, M.; Dai, X.-Y.; Liu, Y. Ultrahigh Supramolecular Cascaded Room-Temperature Phosphorescence Capturing System. *Angew. Chem., Int. Ed.* **2021**, *60*, 27171−27177.
(49) Dai, X.-Y.; Hu, Y.-Y.; Sun, Y.; Huo, M.; Dong, X.; Liu, Y. A Highly Efficient Phosphorescence/Fluorescence Supramolecular Switch Based on a Bromoisoquinoline Cascaded Assembly in Aqueous Solution. *Adv. Sci.* **2022**, *9*, 2200524.
(50) Li, J.-J.; Chen, Y.; Yu, J.; Cheng, N.; Liu, Y. A Supramolecular Artificial Light-Harvesting System with an Ultrahigh Antenna Effect. *Adv. Mater.* **2017**, *29*, 1701905.




https://doi.org/10.1021/acsnano.2c07263
*ACS Nano* 2022, 16, 20559−20566